Optics and Laser Technology 119 (2019) 105592

Contents lists available at ScienceDirect

Optics and Laser Technology

journal homepage: www.elsevier.com/locate/optlastec

Full length article

Factor analysis of selective laser melting process parameters with normalised quantities and Taguchi method

Hua-Zhen Jiang[a,b], Zheng-Yang Li[b,*], Tao Feng[c], Peng-Yue Wu[c], Qi-Sheng Chen[a,b], Yun-Long Feng[c], Shi-Wen Li[c], Huan Gao[a,b], He-Jian Xu[b]

[a] School of Engineering Science, University of Chinese Academy of Sciences, Beijing 100190, China
[b] Institute of Mechanics, Chinese Academy of Sciences, Beijing 100190, China
[c] Beijing E-Plus-3D Technology Co., LTD, Beijing 102299, China

HIGHLIGHTS

- Normalised process map and variables are adopted to determine a processing window.
- ANOVA is used to rank parameters in order of significance on response variables.
- Laser power is a pronounced factor for all the response variables.
- Hardness is strongly affected by porosity and the microstructure of the built part.
- Hatch spacing is more significant than scan speed due to $v_{crit,locl} < v < v_{crit,hacth}$.

ARTICLE INFO

Keywords:
Additive manufacturing
Parameters optimizing
Dimensionless quantities
Selective laser melting
316L stainless steel

ABSTRACT

Extensive experiments have been carried out to derive material-process-microstructure-properties relationships for powder bed fusion (PBF) process. Selecting a set of appropriate processing parameters to achieve high quality part is of great challenge, since the quality of part is affected by many factors involved in the process. However, a lot of investigations of processing parameters on performance of part merely focused on one or two parameters variation while others were fixed. A comprehensive study about the influence of multiple factors on selective laser melting (SLM) process is still lack of deep research. In this paper, normalised quantities, such as E_0^*, q^*, v^*, etc., and a dimensionless group of process variables are adopted to determine a processing window. Taguchi method is used to optimize the settings of processing parameters. Experiments were carried out by SLM with 316 L stainless steel powder. The following response variables, top surface roughness (R_a), hardness (HV) and density (ρ) were measured. The effect of laser power q, scanning speed v, hatch spacing h and their interactions, such as $q \times v$, $q \times h$, $v \times h$, on top surface roughness (R_a), hardness (HV) and density (ρ) was evaluated by Analysis of Variance (ANOVA). It is shown that laser power is of great significance among the parameters, while hatch spacing, scanning speed and their interactions affect the quality of samples with differently significant levels. The results of this research show that normalised processing map is a powerful tool for optimizing processing parameters to get high quality parts.

1. Introduction

Metals can be strengthened by many traditional approaches while compromising ductility and toughness. The strength–ductility trade-off has been a long-standing dilemma in materials science. Recently, several engineered gradient microstructures have been demonstrated to have the potential of achieving both high strength and high ductility [1–3]. However, nearly all these approaches require tooling or surface mechanical treatments, which are not readily applicable to the complex geometry parts necessary for practical applications. Additive manufacturing (AM) is now widely accepted as a new paradigm for the design and production of high performance components for complex structures. Moreover, it provides extensive opportunities to tailor the microstructure and subsequent mechanical properties of the built parts. Wang and Sun [4,5] have reported that 316L stainless steels additively manufactured via a laser powder-bed-fusion technique exhibit a

* Corresponding author.
E-mail address: zyli@imech.ac.cn (Z.-Y. Li).

https://doi.org/10.1016/j.optlastec.2019.105592
Received 27 April 2019; Accepted 20 May 2019
0030-3992/

Nomenclature

A	surface absorptivity (–)
A_0	mass of the sample in the air (kg)
B	total mass of the sample and the support bracket in water (kg)
C	mass of the supporting bracket in water (kg)
C_ρ	specific heat capacity ($J\,kg^{-1}\,K^{-1}$)
CT	correction term (–)
E_0^*	normalized equivalent energy density (–)
K_1	sum of measurement results of each parameter at the level one (–)
K_2	sum of measurement results of each parameter at the level two (–)
K_3	sum of measurement results of each parameter at the level three (–)
L	Length of a single scan vector (m)
Q_T	sum of squares of all the observed data (–)
S_T	total sum of squared deviations (–)
S_e	sum of squared deviation of error (–)
SSm	mean of squared deviations (–)
SSd	sum of squared deviations (–)
T_m	melting temperature (K)
T_0	initial (or powder bed) temperature (K)
d_{diff}	thermal diffusion depth (m)
d	laser beam diameter (m)
h	hatch spacing (m)
h^*	normalised hatch spacing (–)
l	layer thickness (m)
l^*	normalised layer thickness (–)
q	laser power (W)
q^*	normalised power (–)
r_B	laser beam radius (m)
v	scanning speed ($m\,s^{-1}$)
v^*	normalised scanning speed (–)
$v_{crit,local}$	critical scanning speed ($m\,s^{-1}$)
$v_{crit,\ hacth}$	critical hatching speed ($m\,s^{-1}$)
x_i	the observed data for the ith performance characteristics (–)
α	thermal diffusivity or significant level ($m^2\,s^{-1}$ or –)
λ	thermal conductivity ($W\,m^{-1}\,K^{-1}$)
ρ	density of 316L stainless steel ($kg\,m^{-3}$)
ρ_m	the measured density of the sample ($kg\,m^{-3}$)
ρ_0	density of water ($kg\,m^{-3}$)

combination of yield strength and tensile ductility, which surpass those of conventional 316L steels respectively. Their investigations indicate the probability and flexibility of AM technique to tailor microstructures and obtain excellent properties of manufactured part by utilizing specific processing strategies. Numerous investigations have been done to reveal the relationships between the process parameters and the performance of the parts built by AM [6–9]. However, Yadroitsev [10] pointed out that there are more than 130 factors affecting the quality of the parts. To compare results from numerous investigations and to optimize processing parameters, efficient experimental design and analysis method are expected.

Taguchi method with orthogonal array design is a powerful tool for the design of high quality systems. It provides a simple, efficient and systematic approach to optimize designs for quality and cost. The methodology is valuable when the design parameters are qualitative and discrete. However the row and column of orthogonal array are limited. It is almost impossible or unnecessary to investigate all those parameters or most of the parameters within one or a few orthogonal arrays. Dimensional analysis is another powerful tool which can not only reduce the number of parameters that need to be investigated in a multi-variable and complex system, but also compare results from different researches [11–14]. More important, dimensionless parameters have physical meaning, enabling us to investigate which sub-processes are important enough to be investigated further.

In this paper, normalised process map and a dimensionless group of process variables developed by Thomas [15] are adopted to provide an approach for narrowing the range of processing parameters with a consideration of lower normalized energy density. An appropriate orthogonal array is also adopted to study the parameter space with a small number of experiments. Here laser power q, scanning speed v, hatch spacing h and their interactions, such as $q \times v$, $q \times h$, $v \times h$, are selected and evaluated by Analysis of Variance (ANOVA) to rank the order of statistically significance of the parameters on response variables, top surface roughness (R_a), hardness(HV) and density (ρ). The results of this research may help to understand the process-structure-property relationships and to select suitable processing parameters in AM.

2. Experimental procedures

2.1. Design of experiment

Selecting an appropriate set of parameters is a first step for experimental design. It is well known that laser power q, scanning speed v, layer thickness l, hatch spacing h, and scanning pattern are the most important processing parameters during the PBF process [16,17]. A normalized processing diagram has been proposed that synthesizes with various materials and PBF processing parameters. The normalized equivalent energy density E_0^*, which contains all the above parameters, is selected as the basis for designing the experiments. The expression of E_0^* is as follows [15]:

$$E_0^* = \frac{q^*}{v^* l^* h^*} = [Aq/2vlh][1/\rho C_\rho (T_m - T_0)] \quad (1)$$

To summarize and compare the different PBF processings of 316L stainless steel scattering in literatures, the dimensionless processing data calculated from the references [4,18–21] are plotted in Fig. 1(a) with log10 scale of q^*/v^*l^* as abscissa and $1/h^*$ as ordinate, respectively. It is pointed out that higher values of E_0^* represent a combination of process parameters that, overall, lead to excessive heat input into the powder bed, whilst insufficient heat to fully melt or fuse the feedstock powder might be expected at a lower E_0^*. However a constant E_0^* does

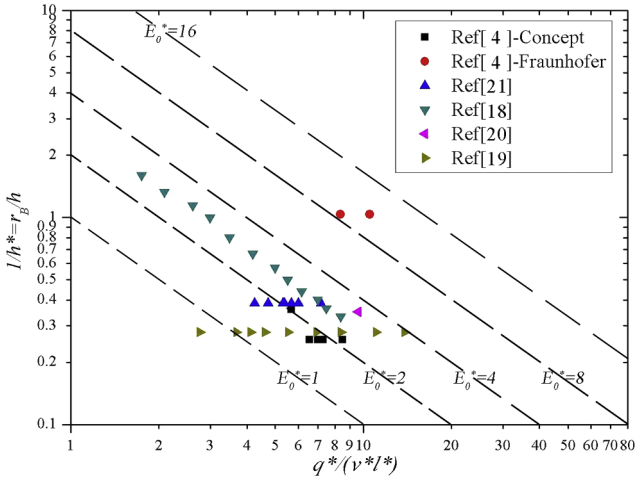

Fig. 1. a. Normalized processing diagram for SLM of 316L stainless steel constructed using E_0^* and the data is extracted from different literatures. Contours of constant normalized equivalent energy density are delineated as dashed lines.

Table 1
Thermo-physical properties of 316L stainless steel.

A[4]	λ(W·m^{-1}·K^{-1})[22]	α(m^{2}s^{-1})[23]	ρ(kg/m^3)	C_p(J·kg^{-1}·K^{-1})[22]	T_m(K)[22]	T_0(K)
0.35	$11.82 + 0.0106T_m$	5.38×10^{-6}	7980	$330.9 + 0.563T_m - 4.015 \times 10^{-4}T_m^2 + 9.465 \times 10^{-8}T_m^3$	1673 K	333 K

Table 2
Factors and levels of the designed experiments.

Levels	Factors		
	$q(q^*)$	$v(v^*)$	$h(h^*)$
1	206 W (45.51)	900 mm/s (6.69)	75 μm (1.88)
2	252 W (55.68)	1100 mm/s (8.18)	90 μm (2.25)
3	298 W (65.84)	1300 mm/s (9.67)	105 μm (2.63)

Note: The dimensionless form of the factor is shown in parenthesis.

not imply the thermal history of a material manufactured that fall somewhere along an isopleth of E_0^* remains the same. Since higher production efficiency and lower energy consumer are always pursued, lower E_0^* is one of the design principles of this study. Considering the limitation of our machine parameters, the parameter selection is firstly confined within the range $2 < q^*/v^*l^* < 10$ and $0.25 < 1/h^* < 1.6$ in this study. The thermo-physical properties of 316L stainless steel used in the experiment are listed in Table 1.

According to the analysis of dimensionless processing data above, the three factors and three levels experiment with the interaction between each other were considered. Laser power q, scanning speed v and hatch spacing h are selected as factors. Three levels are denoted to each factor. With dimensionless form the factors and their levels are shown in Table 2. For an orthogonal array with three factors and three levels, the freedom of each factor and the interaction between each factor can be calculated as $f_q = f_v = f_h = 3–1 = 2$, $f_{q\times v} = f_{v\times h} = f_{h\times q} = 2 \times 2 = 4$. Then, the total number of tests, n should be satisfied as following:

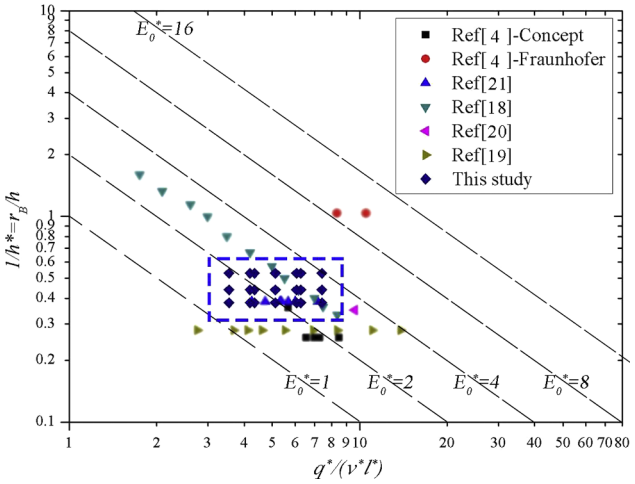

Fig. 1. b. Normalized processing diagram showing the location of the experimental processing parameters selected in this study. The experimental data is inclosed in blue dashed rectangle. (For interpretation of the references to colour in this figure legend, the reader is referred to the web version of this article.)

Table 4
Chemical compositions of as-used 316L stainless steel powder.

Element	Fe	Cr	Ni	Mo	Mn	Si	C	P	S
Content(wt.%)	Bal.	18.84	10.68	2.26	1.05	0.91	⩽0.03	⩽0.04	⩽0.01

Table 3
An orthogonal array L_{27} ($3^{1\,3}$) with factor interactions. E_0^* is denoted to each experiment.

Exp. No.	q	v	$(q \times v)_1$	$(q \times v)_2$	h	$(q \times h)_1$	$(q \times h)_2$	$(v \times h)_1$	$(v \times h)_2$	E_0^*
1	1	1	1	1	1	1	1	1	1	2.808
2	1	1	1	1	2	2	2	2	2	2.340
3	1	1	1	1	3	3	3	3	3	2.006
4	1	2	2	2	1	1	1	2	3	2.297
5	1	2	2	2	2	2	2	3	1	1.914
6	1	2	2	2	3	3	3	1	2	1.641
7	1	3	3	3	1	1	1	3	2	1.944
8	1	3	3	3	2	2	2	1	3	1.620
9	1	3	3	3	3	3	3	2	1	1.388
10	2	1	2	3	1	2	3	1	1	3.435
11	2	1	2	3	2	3	1	2	2	2.862
12	2	1	2	3	3	1	2	3	3	2.453
13	2	2	3	1	1	2	3	2	3	2.810
14	2	2	3	1	2	3	1	3	1	2.342
15	2	2	3	1	3	1	2	1	2	2.007
16	2	3	1	2	1	2	3	3	2	2.378
17	2	3	1	2	2	3	1	1	3	1.982
18	2	3	1	2	3	1	2	2	1	1.698
19	3	1	3	2	1	3	2	1	1	4.062
20	3	1	3	2	2	1	3	2	2	3.385
21	3	1	3	2	3	2	1	3	3	2.901
22	3	2	1	3	1	3	2	2	3	3.323
23	3	2	1	3	2	1	3	3	1	2.769
24	3	2	1	3	3	2	1	1	2	2.374
25	3	3	2	1	1	3	2	3	2	2.812
26	3	3	2	1	2	1	3	1	3	2.343
27	3	3	2	1	3	2	1	2	1	2.008

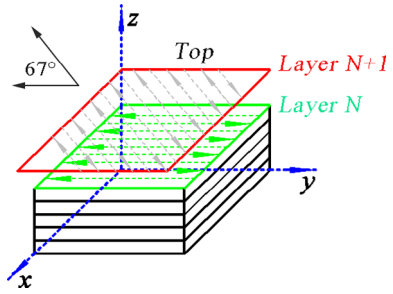

Fig. 2. Scan strategy of this experiment.

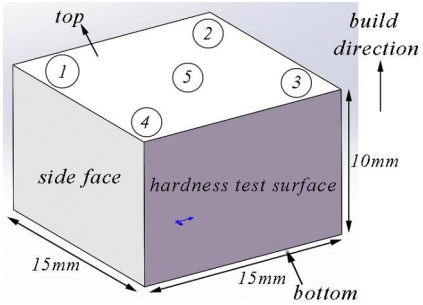

Fig. 3. The sketch of test points on samples.

$n > 1 + f_q + f_v + f_h + f_{q\times v} + f_{v\times h} + f_{h\times q} = 19$,

where f denotes freedom and the subscripts are factors and their interactions. Therefore, the orthogonal array L_{27} (3^{13}) is selected and the interaction between each column of L_{27} (3^{13}) is determined. The experimental scheme is listed in Table 3. Based on the processing map in Fig. 1(a), the normalized parameter groups used in this study are plotted in Fig. 1(b). It is seen that the data of this study is within the range $1 < E_0^* < 4$ and $0.3 < 1/h^* < 0.65$.

2.2. Calculation of ANOVA

The purpose of the analysis of variance (ANOVA) is to investigate which design parameters significantly influence the quality characteristic and to rank the order of statistically significance of the parameters. A tool called *F*-test is used to check which design parameters have a significant effect on the quality characteristic. In performing the *F*-test, the mean of squared deviations *SSm* needs to be calculated. *SSm* is equal to the sum of squared deviations *SSd* divided by the number of degrees of freedom associated with the design parameter. Then, the *F*-value for each design parameter is simply the ratio of the mean of *SSm* to the mean of squared error. Items used in ANOVA are calculated by the following equations:

$$CT = \frac{(\sum_{i=1}^{27} x_i)^2}{27} \tag{2}$$

$$Q_T = \sum_{i=1}^{27} x_i^2 \tag{3}$$

$$S_T = Q_T - CT \tag{4}$$

$$SSd_{(D)} = Q_D - CT \tag{5}$$

$$Q_D = \frac{1}{9}(K_1^2 + K_2^2 + K_3^2) \tag{6}$$

$$S_e = S_T - S_q - S_v - S_h - S_{(q\times v)} - S_{(q\times h)} - S_{(h\times v)} \tag{7}$$

where D represents laser power q, or scanning speed v, or hatch spacing h, or one of their interactions ($q \times v$, $q \times h$, $v \times h$) respectively. Then

Table 5
Results of SLM experiment.

Exp. No.	Factors			R_a (μm)	Density (%)	Hardness(HV_1)
	q^*	v^*	h^*			
1	44.36	6.69	1.88	9.80	99.35	182.38
2	44.36	6.69	2.25	11.65	99.09	229.56
3	44.36	6.69	2.63	10.43	99.04	175.82
4	44.36	8.18	1.88	8.99	99.14	223.26
5	44.36	8.18	2.25	11.55	98.85	186.85
6	44.36	8.18	2.63	10.92	98.31	148.98
7	44.36	9.67	1.88	9.78	98.75	178.46
8	44.36	9.67	2.25	12.22	98.17	147.99
9	44.36	9.67	2.63	11.95	96.84	134.99
10	54.27	6.69	1.88	6.21	99.26	191.99
11	54.27	6.69	2.25	8.43	99.28	211.98
12	54.27	6.69	2.63	9.32	99.29	200.46
13	54.27	8.18	1.88	9.15	99.24	207.06
14	54.27	8.18	2.25	9.67	99.15	224.55
15	54.27	8.18	2.63	6.79	98.99	195.12
16	54.27	9.67	1.88	6.76	99.15	198.96
17	54.27	9.67	2.25	6.65	99.04	181.90
18	54.27	9.67	2.63	5.71	98.40	177.25
19	64.17	6.69	1.88	2.77	99.24	185.33
20	64.17	6.69	2.25	3.82	99.22	197.90
21	64.17	6.69	2.63	4.25	99.17	199.80
22	64.17	8.18	1.88	3.92	99.24	204.88
23	64.17	8.18	2.25	5.40	99.24	198.23
24	64.17	8.18	2.63	10.56	99.11	183.10
25	64.17	9.67	1.88	8.88	99.25	208.72
26	64.17	9.67	2.25	7.11	99.22	197.57
27	64.17	9.67	2.63	7.72	98.76	198.46

$$F = \frac{SSd_{(D)}/f_D}{S_e/f_e} \tag{8}$$

The significance level α was used to determine the significance level. Significance level $\alpha = 0.01$ which can be denoted as $F_{0.01}$ means 99% confidence interval. Different symbols were used to rank the order of significance for these processing parameters. $F > F_{0.01}(f_1, f_2)$ means the factor is pronounced significant and denoted as **; $F_{0.01}(f_1, f_2) \geqslant F > F_{0.05}(f_1, f_2)$ means the factor is significant and denoted as *; $F_{0.05}(f_1, f_2) \geqslant F > F_{0.10}(f_1, f_2)$ means the factor is relatively significant and denoted as (*); $F_{0.10}(f_1, f_2) \geqslant F > F_{0.25}(f_1, f_2)$) means the factor does have an effect but is not significant and denoted as [*]; $F \leqslant F_{0.25}(f_1, f_2)$ means the factor has no effect and denoted as . When the result denoted as the same symbol, the significant order is ranked by *F* value.

2.3. Experimental materials

The chemical compositions of the 316L stainless steel powder are listed in Table 4. The particle size distribution is around 15 ~ 53 μm. The dimension of substrate used in the building process is 246 mm × 246 mm × 40 mm with surface roughness R_a = 1.6 μm. The flatness of substrate is < 35 μm.

2.4. SLM process

Experiment was conducted in EP250 which is equipped with a fiber laser maximum 400 W power and a beam diameter of 80 μm. The oxygen content was maintained below ~1000 ppm during the SLM process. The scanning strategy is illustrated in Fig. 2. The layer thickness is set to be a constant during manufacturing process. The 27 parts under different processing parameters based on Table 3 were fabricated. The dimension of each part is 15 mm × 15 mm × 10 mm shown in Fig. 3.

Table 6
ANOVA of R_a.

Parameter	Sum of square *SSd*	Freedom *f*	Mean square *SSm*	*F*	Significance	F_α
q	105.86	2	52.93	22.43	**	$F_{0.01}(2,16) = 6.23$
v	7.69	2	3.84	1.63	[*]	$F_{0.05}(2,16) = 3.63$
h	8.74	2	4.37	1.85	[*]	$F_{0.1}(2,16) = 2.67$
$q \times v$	30.20	4	7.55	3.20	*	$F_{0.25}(2,16) = 1.51$
$q \times h$	10.91	4	2.73	–		$F_{0.01}(4,16) = 4.77$
$v \times h$	4.18	4	1.04	–		$F_{0.05}(4,16) = 3.01$
e	22.66	8	2.83	–		$F_{0.10}(4,16) = 2.33$
e' ($q \times h$, $v \times h$, e)	37.75	16	2.36	–		$F_{0.25}(4,16) = 1.50$
Total	190.24	26				

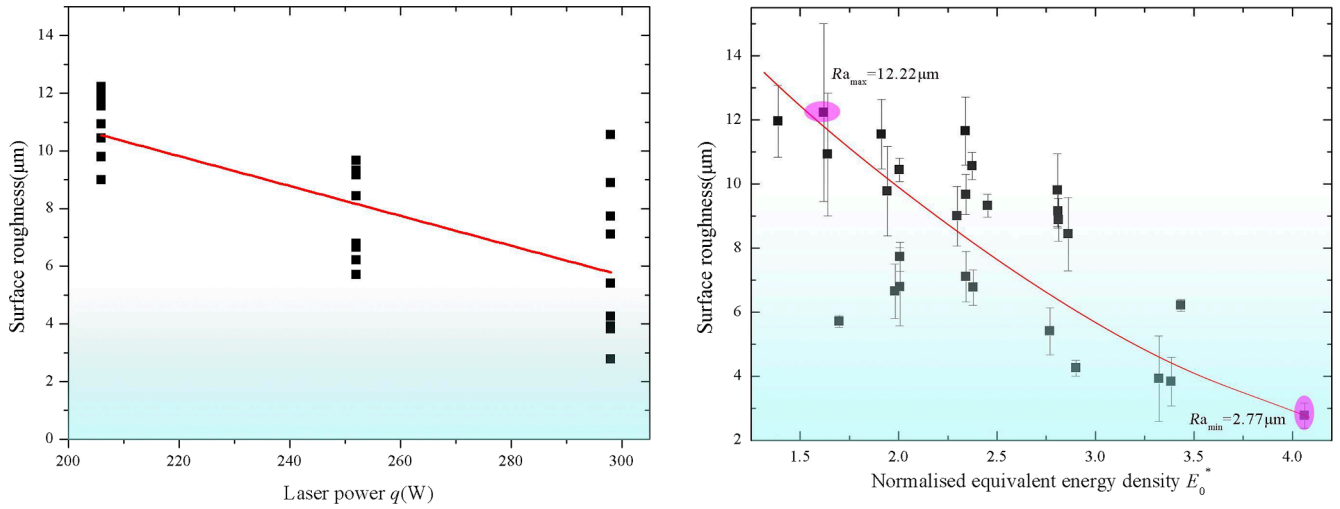

(a) Effect of q on surface roughness R_a (b) Effect of E_0^* on surface roughness R_a

Fig. 4. Effect of laser power and normalised equivalent energy density on surface roughness. (a) Effect of q on surface roughness R_a. (b) Effect of E_0^* on surface roughness R_a.

Table 7
R_a for combination levels of q and v.

v	q		
	q_1	q_2	q_3
v_1	10.63	7.99	3.61
v_2	10.49	8.54	6.63
v_3	11.32	6.37	7.90

2.5. Quality characterization and analysis

Each sample was cut down from the substrate by wire cutting. The side face of all samples were ground using SiC papers from 200 grits up to 3000 grits before being polished using 1.5 μm diamond suspension. The top surface roughness of each sample was measured by surface roughness meter TR200. Five positions on top surface of each sample were selected for measurement (Fig. 3). The density of each additive manufactured sample was measured by high precision electronic densimeter ZMD-2 with Archimedes method. The density (in percentage) for each sample can be estimated as:

$$\frac{\rho_m}{\rho} \times 100\% = \frac{A_0\rho_0}{[A_0 - (B - C)]\rho} \times 100\% \quad (9)$$

Before hardness test the samples were chemically etched in an acidic water solution containing 2% HF and 8% HNO_3 for about 30 min at room temperature. Microstructure characterizations were carried out on the etched surface by Optical Microscopy (OM). The hardness was measured by Everone MH-6 Vickers indenter with a load of 1 kg and dwelling time 20 s. The measurement surface is shown in Fig. 3. At least 7 hardness measurements were taken for each sample and data with the largest deviation in the results was discarded to avoid large experimental errors.

3. Results and discussions

The response variables hardness, surface roughness and density of each sample were measured and the average values were listed on Table 5 according to the experimental numbers on Table 3. It is shown that most of density is higher than 99%, only 1 result of density is lower than 98%. A maximum hardness of 229.56HV_1 is achieved in this study which is a typical value for 316L stainless steel by both Laser Powder Bed Fusion (LPBF) and direct energy deposition (DED) [22,24]. However the surface roughness values are distributed from the range of

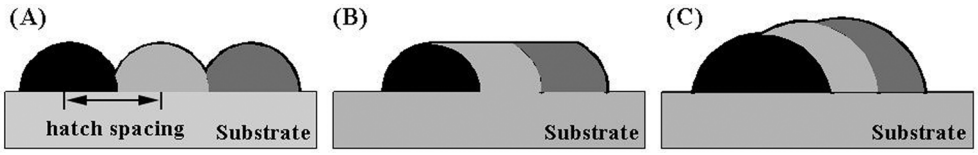

Fig. 5. Schematic diagrams of hatching. (A) The hatch spacing is too large, (B) The hatch spacing is appropriate. (C) The hatch spacing is too small.

Table 8
ANOVA for hardness HV_1.

Parameter	Sum of square *SSd*	Freedom *f*	Mean square *SSm*	*F*	Significance	F_α
q	2238.54	2	1119.27	8.09	*	$F_{0.01}(2,8) = 8.65$
v	1652.05	2	826.025	5.97	*	$F_{0.05}(2,8) = 4.46$
h	2013.23	2	1006.61	7.27	*	$F_{0.10}(2,8) = 3.11$
$q \times v$	2180.22	4	545.05	3.94	*	$F_{0.25}(2,8) = 1.66$
$q \times h$	1365.23	4	341.31	2.47	[*]	$F_{0.01}(4,8) = 7.01$
$v \times h$	2338.92	4	584.73	4.23	*	$F_{0.05}(4,8) = 3.84$
e	1107.06	8	138.38			$F_{0.10}(4,8) = 2.81$
Total	12895.24	26				$F_{0.25}(4,8) = 1.66$

Table 9
Hardness for combination levels of v and h.

h	v		
	v_1	v_2	v_3
h_1	186.57	211.73	195.38
h_2	213.15	203.21	175.82
h_3	192.03	175.73	170.23

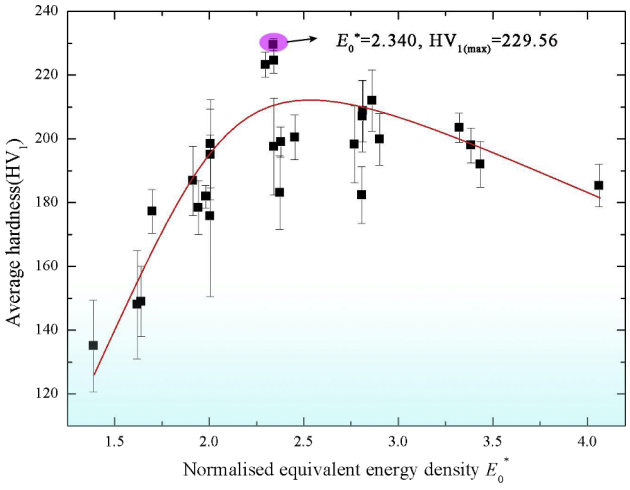

Fig. 6. Effect of normalised equivalent energy density on hardness.

2.77 μm to 12.22 μm. The followings will discuss the experimental results in detail based on the analysis of variance.

3.1. Surface roughness

Table 6 is the result of ANOVA for response variable R_a. Laser power q is pronounced significant on surface roughness R_a since $F_q = 22.43$ far greater than $F_{0.01}$ (2, 16). The significant parameter is the combination of laser power and scanning speed $q \times v$, where $F_{q\times v} = 3.20 > F_{0.05}$ (4, 16). The influence of scanning speed v and hatch spacing h respectively are a little, because the F value of v, of h are a little bit over than that of $F_{0.25}$ (2, 16), where the significance level α is up to 0.25.

Therefore the significance order of parameters on surface roughness is $q > q \times v > h > v$. Fig. 4(a) shows the variation of surface roughness via laser power. The trend of R_a decrease with q increasing, while the distribution of R_a at laser power $q_3 = 298$ W is highly scattering, some R_a values even higher than that of $q_2 = 252$ W. Surface roughness in SLM can be considered as a distribution of final solidified shape of laser melt pool. The melting extent of powder and the state of melt pool is mainly determined by laser power although it is not the only one. Normalized equivalent energy density E_0^* combined several parameters including the major parameter laser power. The variation of R_a via E_0^* is shown in Fig. 4(b). The trend of R_a still decrease with E_0^* increasing although there are some fluctuations among each E_0^*. The fluctuation results from not only the variation of energy input, but also the different thermal history of the material manufactured even under the condition of the same E_0^*. It is revealed that uneven surface and larger surface roughness will occur due to too much energy is input into the melt pool and the surface tension and viscosity of the pool reduce, while insufficient energy input may lead to balling and porosity of melt powder which will also increase surface roughness [25,26]. Ma et al. [27] also pointed out that Marangoni flow was actually beneficial for smoothing the surface roughness when it became dominant in the melt pool with higher energy input. There is an optimal level of input energy density for smooth surface [19]. If the energy density is lower than 104.52 J/mm^3 or over 167.23 J/mm^3, surface roughness is greater than that of 125 J/mm^3. The maximum value of E_0^* is 4.062 in this study. It is smaller than 4.498, the normalized energy input in Ref. [19]. Therefore the situation of Ref. [19] is not occurred in this study.

As a secondary significant factor for surface roughness, it is expected to find out lower R_a value with the best combination level of q and v. Table 7 is the average surface roughness of combination levels of q and v. For instance, 10.63 is the R_a of combination level of q_1 and v_1, which is the average value of all R_a on Table 5 with q_1 and v_1, i. e. the average R_a of No.1, No. 2 and No.3. The lowest R_a on Table 7 is 3.61 which correspond to the combination level of q_3 and v_1, and correspond to that of No. 19, No.20 and No. 21 on Table 5. Thus the best combination of q_3 and v_1 on Table 7 is $q_3v_1h_1$, $R_a = 2.77$, matching on No. 19.

Though the significance of h and v on surface roughness is far lower than that of q and $q \times v$, the results of ANOVA has still shown that h is much significant on R_a than that of v. It may be attribute to the variation of v does not significantly increase or decrease the energy input in this study. The cross section of multiple scanning tracks is sketched in Fig. 5. It is evident that an optimal h between two scanning tracks is existed (Fig. 5 (B)). Whether the hatch spacing is too large (Fig. 5 (A)) or too small (Fig. 5(C)), the surface roughness will increase. The variation of h will change the state of overlapping area between two adjacent tracks. Yadroitsev et al. [28] also pointed out that the interval of stability zone is wider under higher laser power (i.e.50 W) than that of lower power (i.e.25 W), thus scanning speed is insignificant on surface roughness.

3.2. Hardness

All factors except the interaction between laser power and hatch spacing ($q \times h$) are found to be statistically significant for hardness when significance level $\alpha = 0.05$ (Table 8). According to the results of ANOVA, the significance order of parameters on hardness is $q > h > v > v \times h > q \times v$. Since the interaction between scanning speed and hatch spacing is significant when significant level $\alpha = 0.05$, it is necessary to find out the best combination level of v and h. Table 9 is the average hardness of combination levels of v and h. The maximum hardness value on Table 9 is 213.15HV_1 which correspond to the combination level of v_1 and h_2. Thus the best combination in this experiment is $q_2v_1h_2$ which matches No. 11 experiment on Table 5.

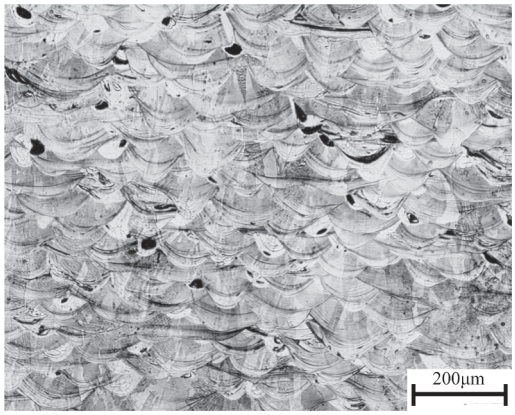

(a) q*=44.36, v*=6.69, h*=1.88 with E_0^*=2.808(corresponding to sample No. 1)

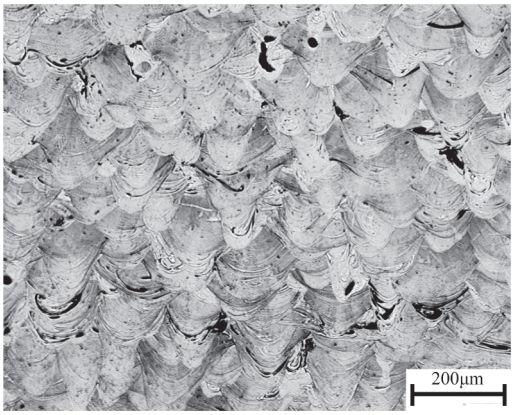

(b) q*=54.27, v*=8.18, h*=1.88 with E_0^*=2.810(corresponding to sample No. 13)

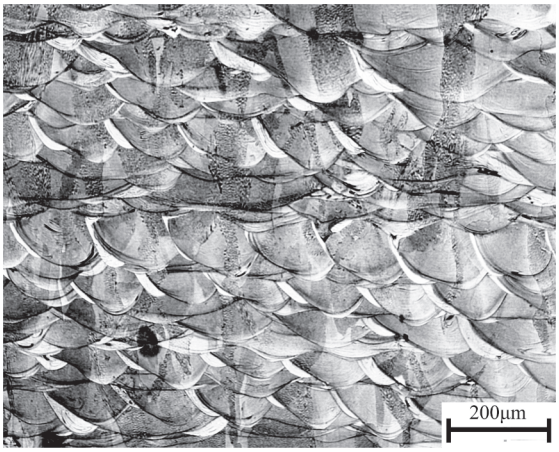

(c) q*=64.17, v*=9.67, h*=1.88 with E_0^*=2.812(corresponding to sample No. 25)

Fig. 7. The cross-section of melt pool with the same E_0^* = 2.81. (a) q^* = 44.36, v^* = 6.69, h^* = 1.88 with E_0^* = 2.808(corresponding to sample No. 1). (b) q^* = 54.27, v^* = 8.18, h^* = 1.88 with E_0^* = 2.810(corresponding to sample No. 13). (c) q^* = 64.17, v^* = 9.67, h^* = 1.88 with E_0^* = 2.812(corresponding to sample No. 25).

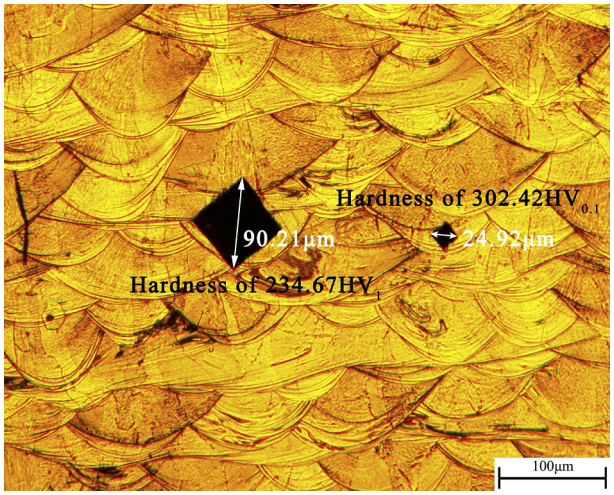

Fig. 8. Typical morphology of indent with the load of 0.1 kg and of 1 kg respectively.

Hardness is depended on the melting extent of powder and the microstructure of the built part for AM. The hardness of the built part may not be so high due to powder is not well-melted and numerous pores left. Fig. 6 shows the variation of hardness via E_0^*. Basically, the trends of hardness firstly increase with E_0^* increasing but decrease if E_0^* greater than about 2.30 though the distribution is relatively scattering for each E_0^*. It can be seen that the error among these measurements for all the samples is larger at lower E_0^*, due to the heterogeneous dispersed porosity and unmelted powder defect. Similar fluctuations could be also found in Ref. [29,30]. It is noted that although a constant E_0* suggests an equally energy efficient process, this does not imply the thermal history of a material manufactured that fall somewhere along an isopleth of E_0^* remains the same [15]. Fig. 7 is the cross-section of melt pool with the same E_0^* = 2.81. It is shown the topographic feature of the melt pool is different not only in size but also in geometry. Thus, the hardness tests with the same E_0^* lead to different hardness. In

Table 10
Thermo-physical properties of 316L SS and processing parameter in SLM.

Parameters	Value	Comment
Thermal diffusion coefficient α($m^2 \cdot s^{-1}$)	5.38×10^{-6}	[23]
★Length of a single scan vector L (m)	$\sim 1.5 \times 10^{-2}$	Experiment data
Thermal diffusion depth d_{diff}(m)	1.2×10^{-4}	4 × layer thickness
Beam diameter d(m)	80×10^{-6}	EP250

★ Due to the scanning strategy in this study is meander with the angle of the laser rotated by 67° between each layer, a single scan vector is different within each layer, so it is reasonable to choose the width of the sample as the characteristic length of a single scan vector.

Table 11
ANOVA for density ρ.

Parameter	Sum of square *SSd*	Freedom *f*	Mean square *SSm*	*F*	Significance	F_α
q	0.000165	2	0.000083	19.77	**	$F_{0.01}(2,8) = 8.65$
v	0.000163	2	0.000082	19.58	**	$F_{0.05}(2,8) = 4.46$
h	0.000128	2	0.000064	15.30	**	$F_{0.10}(2,8) = 3.11$
$q \times v$	0.000100	4	0.000025	5.96	*	$F_{0.25}(2,8) = 1.66$
$q \times h$	0.000053	4	0.000013	3.17	(*)	$F_{0.01}(4,8) = 7.01$
$v \times h$	0.000078	4	0.000019	4.66	*	$F_{0.05}(4,8) = 3.84$
e	0.000033	8	0.000004			$F_{0.10}(4,8) = 2.81$
Total	0.000720	26				$F_{0.25}(4,8) = 1.66$

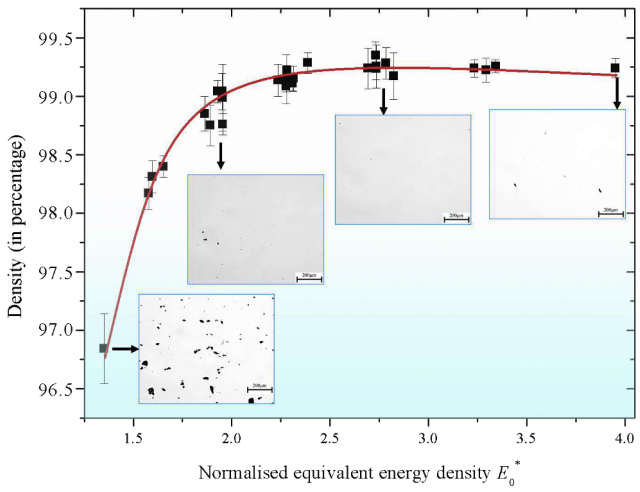

Fig. 9. Effect of normalised equivalent energy density E_0^* on density.

addition, our experimental result is basically consistent with that of Cherry et al. [19]. It indicates that if the energy density is lower than 83.61 J/mm^3 (equivalent to $E_0^* = 2.25$ of this study) or over 125.42 J/mm^3 (equivalent to $E_0^* = 3.37$ of this study), hardness of the build will be < 220HV$_{10}$. It is worth noting that the maximum value of hardness in this study is 229.56HV$_1$ at $E_0^* = 2.340$ which is superior to that of conventional annealed type 316L stainless steel (Type 316 stainless steel, with a hardness between 155 and 170 HV [31]). Furthermore, we also observed that if a load of 0.1 kg carried out by the same Vickers hardness test, the microhardness of the as-SLMed 316L stainless steel sample would be up to 302HV$_{0.1}$, which is comparable to that of Saeidi et al. [32]. Fig. 8 is the typical morphology of indent with the load of 0.1 kg and of 1 kg. It is illustrated that larger load may cover some pores resulting lower hardness. Higher microhardness is obtained in some local area which is corresponding to the processing parameters of this study, although the average hardness of the parts is nearly the same as that of conventionally made.

The microstructure of the part is influenced by the laser energy input to the pool and sequent the solidification rate of the pool. To analyze the effect of hatch spacing h on hardness between adjacent tracks, it is first to distinguish the thermal loss of interaction between laser beam and powder and the thermal loss of which the laser beam returns to the same point at the adjacent line during hatching. The critical scanning speed $v_{crit,\ locl}$ and critical hatching speed $v_{crit,\ hatch}$ are two important criteria [25]. $v_{crit,\ locl}$ is defined as the scanning speed where the interaction time of the powder and the beam (t_{int}) is equal to the time available for diffusion (t_{diff}), $v_{crit,\ hacth}$ is defined as the scanning hatching speed when the return time of the beam (t_{return}) is equal to the time for diffusion (t_{diff}). $v_{crit,local} = \frac{4\times\alpha\times d}{d_{diff}^2}$, where d is the laser beam diameter, d_{diff} is the thermal diffusion depth, α is the thermal diffusivity. $v_{crit,hatch} = \frac{L\times 4\times\alpha}{d_{diff}^2}$, where L is the length of a single scanning vector. If $v > v_{crit,\ locl}$, the energy input by laser doesn't have enough time to diffuse, and the local thermal loss can be neglected. If $v > v_{crit,\ hacth}$, the next laser scanning is return so quickly that the energy input by the adjacent laser accumulated. According to the thermo-physical properties of 316L stainless steel and processing parameters listed on Table 10, $v_{crit,\ locl}$ and $v_{crit,\ hacth}$ are calculated as following.

$$v_{crit,local} = \frac{4\times\alpha\times d}{d_{diff}^2} = \frac{4\times 5.38\times 10^{-6}\times 80\times 10^{-6}}{(1.2\times 10^{-4})^2} \approx 0.12 m/s$$

$$v_{crit,hatch} = \frac{L\times 4\times\alpha}{d_{diff}^2} = \frac{1.5\times 10^{-2}\times 4\times 5.38\times 10^{-6}}{1.2^2\times 10^{-8}} \approx 22.42 m/s$$

The maximum scanning speed in our study is 1.30 m/s, much greater than $v_{crit,\ locl}$, but much smaller than $v_{crit,\ hacth}$. Therefore the local thermal loss can be neglected but the adjacent laser energy is not accumulated. The influence of scanning speed on local thermal loss is less than that of hatching space. It is revealed that the energy accumulation had a great influence on the heat flow direction and the mean primary dendrite spacing, and this in turn would affect hardness of the part [29].

3.3. Density

Table 11 shows that all factors except the interaction between laser power and hatch spacing ($q \times h$) have significant effect on density when significance level $\alpha = 0.05$. According to the results of ANOVA, the significance order of parameters on density is $q > v > h > q \times v > v \times h$. The F value of q and of v is almost the same which means they have equal significance on density. Fig. 9 shows the variation of density via normalized equivalent energy density E_0^*. The trends of density firstly increase with E_0^* increasing but slightly decrease if E_0^* greater than about 2.80. At low normalised equivalent energy density E_0^*, both large porosity with irregular shape and small spherical pores are observed (Fig. 10(a), (b)), while at higher energy density, vertical cracks spanning several melt pools are formed (Fig. 10(c), (d)). Such vertical cracks may be due to greater penetration depth, keyhole effect and higher thermal gradient caused by slow scan speed [18]. In addition, improper melting mostly between two adjacent melt pool boundaries is also observed (Fig. 10(e), (f)). The result is basically consistent with that of Cherry et al. [19] where the minimum porosity was obtained at energy density 104.52 J/mm^3 which is equivalent to the normalized energy density 2.81 of this study.

Numerical simulation based on a simple Eagar-Tsai model also revealed that laser power and scanning speed had greater effect than other parameters such as beam diameter and absorptivity [21]. However, the variation in scanning speed mainly affects the energy input per unit time which further affects the density of the part. If the scanning speed is too slow, keyhole effect will occur [23], while improper melting such as lack of fusion defects will occur if the scanning speed is too fast [33]. It is pointed out that under the condition of suitable laser power and scanning speed, the powder can be melted well without affecting the building process unless the hatch spacing exceeds the

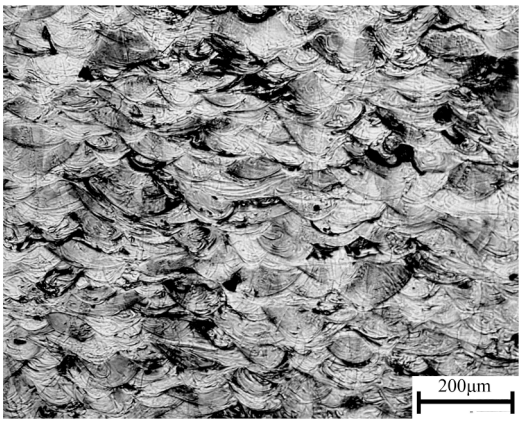

(a) Low magnification OM micrograph of sample No. 9, E_0^*=1.388

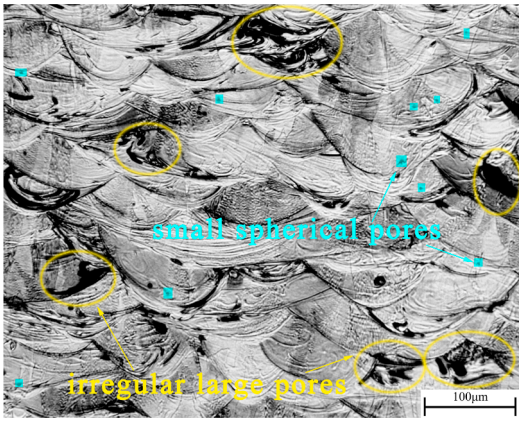

(b) High magnification OM micrograph of sample No. 9, E_0^*=1.388

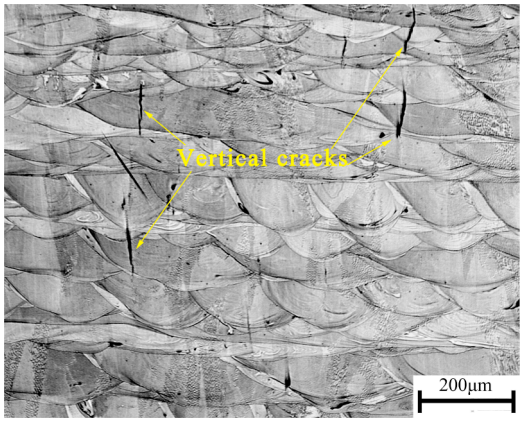

(c) Low magnification OM micrograph of sample No. 22, E_0^*=3.323

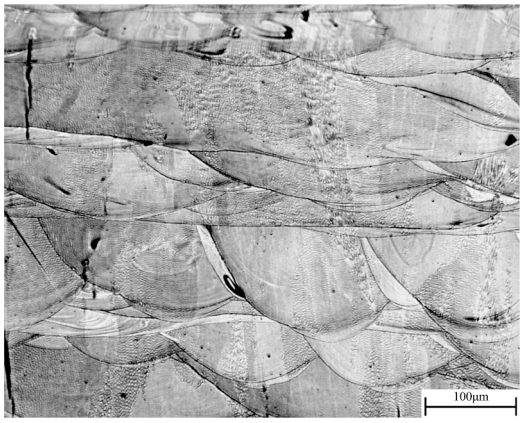

(d) High magnification OM micrograph of sample No. 22, E_0^*=3.323

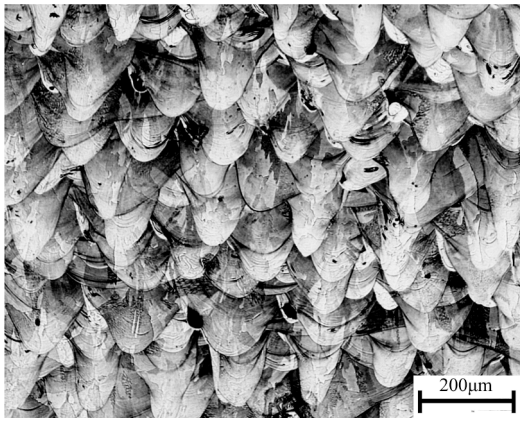

(e) Low magnification OM micrograph of sample No. 19, E_0^*=4.062

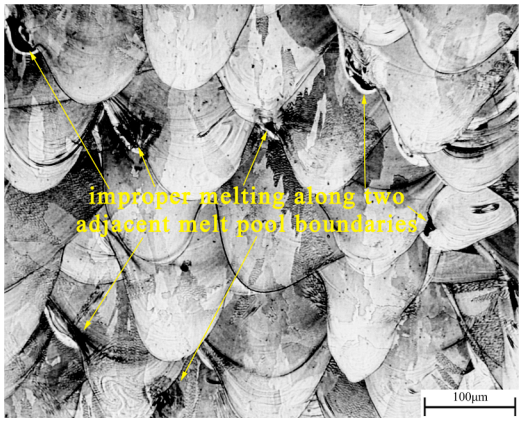

(f) High magnification OM micrograph of sample No. 19, E_0^*=4.062

Fig. 10. OM micrographs showing pores, vertical cracks and improper melting observed. (a) Low magnification OM micrograph of sample No. 9, E_0^* = 1.388. (b) High magnification OM micrograph of sample No. 9, E_0^* = 1.388. (c) Low magnification OM micrograph of sample No. 22, E_0^* = 3.323. (d) High magnification OM micrograph of sample No. 22, E_0^* = 3.323. (e) Low magnification OM micrograph of sample No. 19, E_0^* = 4.062. (f) High magnification OM micrograph of sample No. 19, E_0^* = 4.062.

width of a single vector [28]. Thus hatch spacing is widely adjusted if energy input is sufficient. The result implies that h is less influence than v on density.

For high density, it is expected to find out the best combination level of q and v. The highest density on Table 12 is 99.28% which correspond to the combination q_2v_1. It means that the best combination of q_2 and v_1 in this experiment is $q_2v_1h_1$, which matches No. 10 experiment on Table 5.

Table 12
Density for combination levels of q and v.

v	q		
	q_1	q_2	q_3
v_1	99.16%	99.28%	99.21%
v_2	98.73%	99.12%	99.20%
v_3	97.92%	98.86%	99.08%

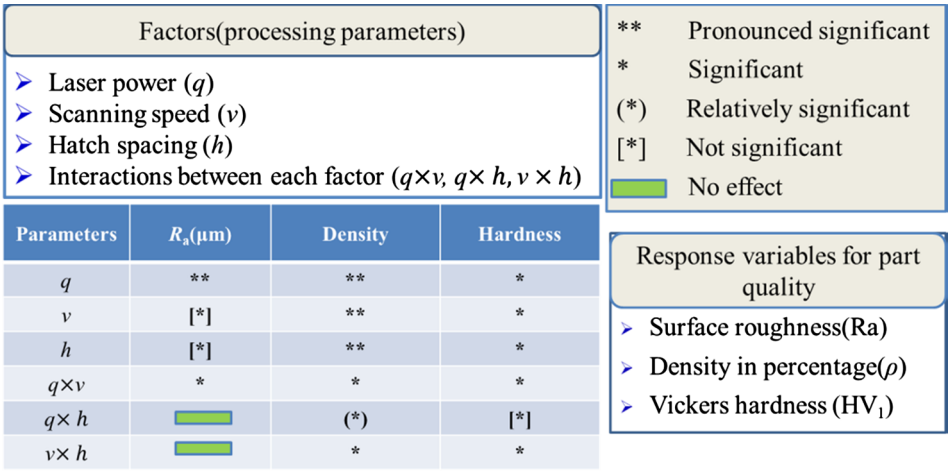

Fig. 11. Summary of the significance order for response variables.

4. Conclusions

Normalised processing diagram was used in this paper to narrow the range of processing parameters. With the experimental design of orthogonal array and ANOVA, the order of significance of processing parameters, such as q, v, h and their interactions on response variables, top surface roughness, density and hardness of additive manufactured 316L stainless steel is shown in Fig. 11. It is concluded that laser power is a pronounced factor for all the response variables. The conclusions are summarized as follows:

(1) For top surface roughness, the significance order is $q > q \times v > h > v$. Balling and Marangoni flow are strongly influenced by normalised energy density, and it in turn affects top surface roughness. The surface roughness generally decreases with the increasing E_0^* and reaches a minimum value of 2.77 μm when $E_0^* = 4.062$.
(2) For density, the significance order is $q > v > h > q \times v > v \times h$. The result implies that influence of hatch spacing h is less than scanning speed v on density due to hatch spacing is widely adjusted under sufficient energy input. In addition, the highest density is 99.35% with a normalised equivalent energy density $E_0^* = 2.808$.
(3) For hardness, the significant order is $q > h > v > v \times h > q \times v$. Hardness is strongly affected by porosity and the microstructure of the built part. Hatch spacing h is more significant than scan speed v attributed to scanning speed is much greater than $v_{crit,\ locl}$, while much smaller than $v_{crit,\ hacth}$, the local thermal loss can be neglected but the adjacent laser energy is not accumulated. Furthermore, the experimental result shows that the hardness reaches a maximum value of 229.56HV_1 when $E_0^* = 2.340$.

Acknowledgements

This work has been supported by the National Natural Science Foundation of China (Grant No. 11772344) and National Key R&D Program of China (Project No. 2016YFB1100700).

References

[1] T.H. Fang, W.L. Li, N.R. Tao, K. Lu, Revealing extraordinary intrinsic tensile plasticity in gradient nano-grained copper, Science 331 (6024) (2011) 1587–1590.
[2] Y. Wei, Y. Li, L. Zhu, Y. Liu, X. Lei, G. Wang, Y. Wu, Z. Mi, J. Liu, H. Wang, Evading the strength-ductility trade-off dilemma in steel through gradient hierarchical nanotwins, Nature Commun. 5 (4) (2014) 3580.
[3] X. Wu, M. Yang, F. Yuan, G. Wu, Y. Wei, X. Huang, Y. Zhu, Heterogeneous lamella structure unites ultrafine-grain strength with coarse-grain ductility, Proc. Natl. Acad. Sci. U S A 112 (47) (2015) 14501.
[4] Y.M. Wang, T. Voisin, J.T. McKeown, J. Ye, N.P. Calta, Z. Li, Z. Zeng, Y. Zhang, W. Chen, T.T. Roehling, R.T. Ott, M.K. Santala, P.J. Depond, M.J. Matthews, A.V. Hamza, T. Zhu, Additively manufactured hierarchical stainless steels with high strength and ductility, Nature Mater. 17 (1) (2018) 63–71.
[5] Z.J. Sun, X.P. Tan, S.B. Tor, C.K. Chua, Simultaneously enhanced strength and ductility for 3D-printed stainless steel 316L by selective laser melting, Npg Asia Mater. 10 (4) (2018) 127.
[6] L.N. Carter, C. Martin, P.J. Withers, M.M. Attallah, The influence of the laser scan strategy on grain structure and cracking behaviour in SLM powder-bed fabricated nickel superalloy, J. Alloys Compounds 615 (2) (2014) 338–347.
[7] M. Gäumann, C. Bezençon, P. Canalis, W. Kurz, Single-crystal laser deposition of superalloys: processing–microstructure maps, Acta Mater. 49 (6) (2001) 1051–1062.
[8] Y. Zhong, L.F. Liu, S. Wikman, D.Q. Cui, Z.J. Shen, Intragranular cellular segregation network structure strengthening 316L stainless steel prepared by selective laser melting, J. Nucl. Mater. 470 (2016) 170–178.
[9] C. Qiu, M. Al Kindi, A.S. Aladawi, I. Al Hatmi, A comprehensive study on microstructure and tensile behaviour of a selectively laser melted stainless steel, Sci. Rep. 8 (1) (2018) 7785.
[10] I. Yadroitsev, Selective laser melting: direct manufacturing of 3D-objects by selective laser melting of metal powders, LAP Lambert Academic Publishing, Germany, 2009 PhD thesis.
[11] J.C. Ion, H.R. Shercliff, M.F. Ashby, Diagrams for laser materials processing, Acta Metallurgica Et Materialia 40 (7) (1992) 1539–1551.
[12] F. Al-Bender, J.P. Kruth, M.V. Elsen, Application of dimensional analysis to selective laser melting, Rapid Prototyping J. 14 (1) (2008) 15–22.
[13] T. Mukherjee, V. Manvatkar, A. De, T. DebRoy, Dimensionless numbers in additive manufacturing, J. Appl. Phys. 121 (6) (2017) 064904.
[14] T. Mukherjee, J.S. Zuback, A. De, T. DebRoy, Printability of alloys for additive manufacturing, Sci. Rep. 6 (2016) 19717.
[15] M. Thomas, G.J. Baxter, I. Todd, Normalised model-based processing diagrams for

additive layer manufacture of engineering alloys, Acta Materialia 108 (2016) 26–35.
[16] J.P. Kruth, M. Badrossamay, E. Yasa, J. Deckers, L. Thijs, J. Van Humbeeck, Part and material properties in selective laser melting of metals, Proceedings of the 16th international symposium on electromachining, (ISEM XVI), Shanghai, (2010).
[17] E. Yasa, T. Craeghs, M. Badrossamay, J.P. Kruth, Rapid manufacturing research at the catholic University of Leuven, US-TURKEY workshop on rapid technologies, Istanbul, (2009).
[18] Z.J. Sun, X.P. Tan, S.B. Tor, W.Y. Yeong, Selective laser melting of stainless steel 316L with low porosity and high build rates, Mater. Des. 104 (2016) 197–204.
[19] J.A. Cherry, H.M. Davies, S. Mehmood, N.P. Lavery, S.G.R. Brown, J. Sienz, Investigation into the effect of process parameters on microstructural and physical properties of 316L stainless steel parts by selective laser melting, Int. J. Adv. Manuf. Technol. 76 (5–8) (2015) 869–879.
[20] K. Saeidi, X. Gao, Y. Zhong, Z.J. Shen, Hardened austenite steel with columnar sub-grain structure formed by laser melting, Mater. Sci. Eng. 625 (2015) 221–229.
[21] C. Kamath, B. El-dasher, G.F. Gallegos, W.E. King, A. Sisto, Density of additively-manufactured, 316L SS parts using laser powder-bed fusion at powers up to 400 W, Int. J. Adv. Manuf. Technol. 74 (1–4) (2014) 65–78.
[22] T. Debroy, H.L. Wei, J.S. Zuback, T. Mukherjee, J.W. Elmer, J.O. Milewski, A.M. Beese, A. Wilson-Heid, A. De, W. Zhang, Additive manufacturing of metallic components – process, structure and properties, Progress Mater. Sci. 92 (2017).
[23] W.E. King, H.D. Barth, V.M. Castillo, G.F. Gallegos, J.W. Gibbs, D.E. Hahn, C. Kamath, A.M. Rubenchik, Observation of keyhole-mode laser melting in laser powder-bed fusion additive manufacturing, J. Mater. Proc. Technol. 214 (12) (2014) 2915–2925.
[24] P. Krakhmalev, G. Fredriksson, K. Svensson, I. Yadroitsev, I. Yadroitsava, M. Thuvander, R. Peng, Microstructure, solidification texture, and thermal stability of 316 l stainless steel manufactured by laser powder bed fusion, Metals 8 (8) (2018) 643.
[25] V. Juechter, T. Scharowsky, R.F. Singer, C. Körner, Processing window and evaporation phenomena for Ti–6Al–4V produced by selective electron beam melting, Acta Materialia 76 (9) (2014) 252–258.
[26] D. Gu, Y. Shen, Effects of processing parameters on consolidation and microstructure of W-Cu components by DMLS, J. Alloys Comp. 473 (1) (2009) 107–115.
[27] C. Ma, M. Vadali, N.A. Duffie, F.E. Pfefferkorn, X. Li, Melt pool flow and surface evolution during pulsed laser micro polishing of Ti_6Al_4V, J. Manufact. Sci. Eng. (2013).
[28] I. Yadroitsev, P. Bertrand, I. Smurov, Parametric analysis of the selective laser melting process, Appl. Surf. Sci. 253 (19) (2007) 8064–8069.
[29] D. Wang, C.H. Song, Y.Q. Yang, Y.C. Bai, Investigation of crystal growth mechanism during selective laser melting and mechanical property characterization of 316L stainless steel parts, Mater. Des. 100 (2016) 291–299.
[30] M. Ziętala, T. Durejko, M. Polański, I. Kunce, T. Płociński, W. Zieliński, M. Łazińska, W. Stępniowski, T. Czujko, K.J. Kurzydłowski, The microstructure, mechanical properties and corrosion resistance of 316 L stainless steel fabricated using laser engineered net shaping, Mater. Sci. Eng.: A 677 (2016) 1–10.
[31] D. Aylor, Evaluating erosion corrosion, cavitation, and impingement, corrosion: fundamentals, testing, and protection, ASM Handbook, ASM International, 2003, pp. 639–643.
[32] K. Saeidi, X. Gao, F. Lofaj, L. Kvetková, Z.J. Shen, Transformation of austenite to duplex austenite-ferrite assembly in annealed stainless steel 316L consolidated by laser melting, J. of Alloys Comp. 633 (2015) 463–469.
[33] L. Cla, S. Marussi, R.C. Atwood, M. Towrie, P.J. Withers, P.D. Lee, In situ X-ray imaging of defect and molten pool dynamics in laser additive manufacturing, Nature Commun. 9 (1) (2018) 1355.